Heavy air pollution with the unique "non-stagnant" atmospheric boundary layer in the Yangtze River Middle Basin aggravated by regional transport of $PM_{2.5}$ over China

Chao Yu[1,2], Tianliang Zhao[1,*], Yongqing Bai[3,*], Lei Zhang[1,4], Shaofei Kong[5], Xingna Yu[1], Jinhai He[1], Chunguang Cui[3], Jie Yang[1], Yinchang You[1], Guoxu Ma[1], Ming Wu[1], Jiacheng Chang[1]

1 Collaborative Innovation Center on Forecast and Evaluation of Meteorological Disasters, Key Laboratory for Aerosol-Cloud-Precipitation of China Meteorological Administration, PREMIC, Nanjing University of Information Science and Technology, Nanjing 210044, China

2 Southwest Electric Power Design Institute Co., Ltd of China Power Engineering Consulting Group, Chengdu, 610021, China

3 Institute of Heavy Rain, China Meteorological Administration, Wuhan, 430205, China

4 Chengdu Academy of Environmental Sciences, Chengdu, 610031, China

5 Department of Atmospheric Sciences, School of Environmental Studies, China University of Geosciences (Wuhan), 430074, Wuhan, China

Correspondence: Tianliang Zhao (tlzhao@nuist.edu.cn); Yongqing Bai (2007byq@163.com)

Abstract: Regional transport of air pollutants controlled by both emission sources and meteorological factors results in a complex source-receptor relationship of air pollution change. Wuhan, a metropolis in the Yangtze River Middle Basin (YRMB) of Central China experienced heavy air pollution characterized by hourly $PM_{2.5}$ concentrations reaching 471.1 μg m^{-3} in January 2016. In order to investigate the regional transport of $PM_{2.5}$ over Central and Eastern China (CEC) and the meteorological impact on wintertime air pollution in the YRMB area, observational meteorological and other relevant environmental data from January 2016 were analyzed. Our analysis presented the noteworthy cases of heavy $PM_{2.5}$ pollution in the YRMB area with the unique "non-stagnant" meteorological conditions of strong northerly winds, no temperature inversion and additional unstable structures in the atmospheric boundary layer. This unique set of conditions differed from the stagnant meteorological conditions characterized by near-surface weak winds, air temperature inversion, and stable structure in the boundary layer observed in heavy air pollution over most regions in China. The regional transport of $PM_{2.5}$ over CEC aggravated $PM_{2.5}$ levels for heavy air pollution present in the YRMB area, thus demonstrating the source-receptor relationship between the originating air pollution regions in CEC and the receiving YRMB regions. Furthermore, a backward trajectory simulation using FLEXPART-WRF to integrate the air pollutant emission inventory over China was used to explore the patterns of regional transport of $PM_{2.5}$ governed by the strong northerly winds in the cold air activity of the East Asian winter monsoon over CEC, which contributes markedly to the heavy $PM_{2.5}$ pollution in the YRMB area. It was estimated that the regional transport of $PM_{2.5}$ from non-local air pollutant emissions could contribute more than 65% of the $PM_{2.5}$ concentrations to the heavy air pollution in the YRMB region during the study period, revealing the importance of the regional transport of air pollutants over China in the formation of heavy air pollution over the YRMB area.

Key words: $PM_{2.5}$ pollution; Yangtze River Middle Basin; meteorological condition; regional transport; FLEXPART-WRF

1. Introduction

Haze pollution could result in serious environmental problems with adverse influence on traffic, human health, climate change and other significant aspects (An et al., 2019; Fuzzi et al., 2015; Nel, 2005). Based on the observations in China, there is a well-established association between haze pollution and high concentrations of $PM_{2.5}$ (particulate matter with an aerodynamically diameter equal to or less than 2.5 μm). Air pollution levels are highly dependent on emissions of air pollutants and changes in meteorology (An et al., 2019; Tie et al., 2017; Xu et al., 2016a; Xu et al., 2016b). The accumulation, maintenance and dissipation of haze pollution events are generally determined by meteorological changes (Zhang et al., 2013; Zhang et al., 2015), among which the boundary layer structures play the most important role (Zhao et al., 2013). Meteorological conditions of stagnation characterized by near-surface low winds, high humidity and stable boundary layer could govern the periodic variations of haze pollution, which present as typical wintertime air pollution in China (Huang et al., 2018; Xu et al., 2016b; Zhang et al., 2013). The major anthropogenic pollutant sources exist over the vast flatland in Central and Eastern China (CEC) from the eastern edges of the Tibetan Plateau and the Loess Plateau to China's Pacific coast, where four major regions of emission sources exhibiting haze pollution with excessive $PM_{2.5}$ concentrations and overall poor air quality are centered over North China Plain (NCP), Yangtze River Delta (YRD) in East China, Pearl River Delta (PRD) in South China and Sichuan Basin (SCB) in Southwest China, and severe haze pollution events swept over much of CEC-region attributed by regional transport of air pollutants in recent years (Cheng et al., 2008; Deng et al., 2011; Qiao et al., 2019; Tie et al., 2017; Wang et al., 2016; Zhang et al., 2012). Regional transport of air pollutants with the source-receptor relationship is an important issue in our understanding of changes in air quality.

The source-receptor relationship of air pollution describes the impacts of emissions from an upwind source region to pollutant concentrations or deposition at a downwind receptor area (Seibert and Frank, 2004). Regional transport of source-receptor air pollutants is generally complicated by two types of factors: emission and meteorology (Voulgarakis et al., 2010; Zhao et al., 2012). The emission factor includes the emission source strength, chemical transformation and production; the meteorological factor determines the transport pathway from the source to receptor regions, exchanges between boundary layer and free troposphere, the removal processes occurring over the source and receptor regions as well as along the transport pathways. Driven by atmospheric circulations, the regional transport of $PM_{2.5}$ from source regions can deteriorate air quality in the downwind receptor regions, leading to the regional haze pollution observed in a large area over China (Chang et al., 2018; He et al., 2017; Hu et al., 2018; Jiang et al., 2015; Wang et al., 2014).

The Yangtze River Middle Basin (YRMB) covering the lower subbasin of two provinces Hubei and Hunan in Central China is geographically surrounded by four major haze pollution regions in all directions with NCP to the north, the YRD to the east, the PRD to the south and the SCB to the west (see Fig.1a). Due to this specialized location of YRMB as a regional air pollutant transport hub with subbasin topography (see Fig. 1b), the regional transport of air pollutants driven by the cold air flows of East Asian winter monsoonal winds over CEC could build a special source-receptor relationship between the source regions of haze pollution in upstream NCP, YRD, etc. and the downwind YRMB region (Zhong et al., 2019). However, there are unresolved questions regarding the meteorological processes involved in the regional transport of air pollutants and the pattern of regional transport over CEC with contribution to the air pollution changes observed in the YRMB area for the special source-receptor relationship.

Wuhan, a metropolis located in the YRMB, has confronted the environmental problems associated with urban air pollution, especially heavy $PM_{2.5}$ pollution events that occur frequently in the winter (Gong et al., 2015; Xu et al., 2017). Local emissions of air pollutants from urban transportation, industrial exhaust and bio-combustion play an important role in YRMB urban air pollution (Acciai et al., 2017; Zhang et al., 2015). Previous observational and modeling studies on air pollution in this urban area have been conducted (Wu et al., 2018; Zheng et al., 2019). However, regional transport routes of $PM_{2.5}$ across CEC governed by meteorological drivers and their contribution to air pollution over the YRMB area have been poorly understood, especially in relation to heavy air pollution episodes. This study selected Wuhan as a representative area within the YRMB for investigating the meteorological changes of air pollution events in January 2016 and assessing the contribution of regional transport of $PM_{2.5}$ over CEC to heavy air pollution in the YRMB area.

2. Data and methods

2.1 Data

Wuhan, the capital of Hubei province, is located across the Yangtze River, where its surrounding water network attributed with a humid environment (see Fig. 1b). In order to analyze air quality change in Wuhan, the hourly concentrations of air pollutants including $PM_{2.5}$ in January 2016 were collected from the national air quality monitoring network operated by the Ministry of ecology and environmental protection of China (http://www.mee.gov.cn/), including ten observational sites in Wuhan with nine urban sites in residential and industrial zones as well as one suburban site (Fig. S1). The mass concentrations of surface $PM_{2.5}$ are operationally hourly observed with the instrument of the Thermo Fisher Scientifi. The observation data of air quality are released by the Ministry of ecology and environmental protection of China under quality control based on the China's national standard of air quality observation.

The surface $PM_{2.5}$ concentrations averaged over the ten observational sites in Wuhan were used to characterize the variations of air pollution in January 2016 over this YRMB urban area. The correlation coefficients were calculated between the 10-site averages of $PM_{2.5}$ concentrations and the observed meteorological elements (wind speed, air temperature etc.) in Wuhan over January 2016 to explore the local meteorological influences on the changes of ambient $PM_{2.5}$ concentrations in the YRMB area.

The meteorological data of surface observation and air sounding in Wuhan and other observatories in CEC were obtained from the Meteorological Data Sharing Network of China Meteorological Administration (http://data.cma.cn/). Meteorological data selected for this study included air temperature, relative humidity, air pressure, and wind speed and wind direction with temporal resolutions of 3 h for surface observation and 12 h for sounding observation in order to analyze the meteorological variations in the atmospheric boundary layer in January 2016.

The ERA (ECMWF ReAnalysis) -Interim reanalysis data of meteorology from the ECMWF (European Centre for Medium-Range Weather Forecasts) (https://www.ecmwf.int/en/forecasts/datasets/reanalysis-datasets/) were applied to explore the cold air flows of East Asian winter monsoonal winds in January 2016 and their anomalies during heavy

$PM_{2.5}$ pollution over the CEC region.

2.2 FLEXPART-WRF modeling

2.2.1 Model description

The Flexible Particle dispersion (FLEXPART) model (Stohl et al., 2003; Stohl et al., 2005) is a Lagrange particle diffusion model developed by the Norwegian Institute for Air Research (NIAR). In this model, the trajectory of a large number of particles released from a source is simulated with consideration of the processes of tracer transport, turbulent diffusion, and wet and dry depositions in the atmosphere (Brioude et al., 2013). Applying backward trajectory simulation can determine the distribution of potential source regions that may have an impact on a target point or receptor region (Chen et al., 2017a; Chen et al., 2017b; Seibert and Frank, 2004; Zhai et al., 2016).

Initially, FLEXPART could be driven by the global reanalysis meteorological data obtained from the ECMWF or the National Centers of Environmental Prediction (NCEP). In this study on the fine and multiscale modeling of air pollutant sources and regional transport, FLEXPART was coupled offline with the Weather Research and Forecasting Model (WRF) to effectively devise the combined model FLEXPART-WRF (Fast and Easter, 2006; Brioude et al., 2013), which has been widely used to investigate the potential sources of air pollutants in consideration of environmental change (An et al., 2014; De Foy et al., 2011; Sauvage et al., 2017; Stohl et al., 2003).

2.2.2 WRF modeling configuration and validation

The WRF model was configured with two nested domains in this study. The coarse domain covered the entirety of Asia with a 30 km×30 km horizontal resolution, and the nested fine domain included most of China and surrounding regions with a 10 km×10 km horizontal resolution (Fig. S2). The physical parameterizations used in WRF modeling were selected with the Morrison microphysics scheme (Morrison et al., 2009), the Rapid Radiative Transfer Model (RRTM) scheme for long and short wave radiation (Mlawer et al., 1997), the Yonsei University (YSU) boundary layer scheme (Hong et al., 2006), Grell 3D cumulus parameterization, and the Noah land surface scheme (Grell et al., 2005). Driven with the reanalysis meteorological data in the horizontal resolutions of 1°×1° obtained from NCEP for initial and boundary meteorological conditions, the WRF simulation ran 12 h each time with the first 6 h simulations constituting spin-up time.

The WRF-simulated meteorological fields, which included wind speed, wind direction, air temperature, relative humidity and surface pressure, were compared with observations at five typical sites (Wuhan, Changsha, Hefei, Zhengzhou and Nanchang) over CEC. The correlation coefficients and normalized standardized deviations were calculated and shown in Figure 2 (Taylor, 2001). Based on the results with correlation coefficients passing the significance level of 0.001 and low normalized standardized deviations (Fig. 2), it was evaluated that WRF-modeled meteorology was reasonably consistent with observations and could be used to drive the FLEXPART backward trajectory simulation in this study.

2.3 Estimating contribution of regional transport of $PM_{2.5}$ to air pollution

In the model FLEXPART-WRF, the trajectory of a large number of particles released from a source is simulated with consideration of the processes of tracer transport, turbulent diffusion, wet and dry depositions in the atmosphere. With Lagrangian method, it could result in a Jacobian matrix (footprint), in unit of mass per volume per unit flux. Stohl et al (2005) mathematically derived the residence time for particles out of FLEXPART. Generally, in the backward trajectory of FLEXPART modeling, a large number of particles is released at a receptor and transported backward in time. Then the residence time (not the lifetime) of all particles, normalized by the total number of released particles, is determined on a uniform grid. In this study for the receptor of Wuhan in the YRMB, the residence time for a thickness of 100 m above the surface was calculated and considered the ‘‘footprint’’ (in unit of s). By multiplying the residence time with the air pollutant emission flux in the respective grid cell (in unit of μg m^{-2} s^{-1}) calculated from the air pollutant emission inventory of year 2016 for China (http://www.meicmodel.org/), the emission source contribution (in μg m^{-2}) from this grid cell to the receptor's air pollution change could be estimated(Stohl et al., 2003; Stohl et al., 2005; Ding et al., 2009).

In this study, the FLEXPART-WRF simulation was conducted for the 48-hr backward trajectory with a release of 50,000 air particles at first hour in Wuhan (30.61 ° N, 114.42 ° E) respectively for three heavy pollution events during January 2016. The 48-hr backward trajectory simulation results were output with the residence time of air particles in a horizontal resolution of 0.1°×0.1°. The simulations of particle residence time over the 48-hr backward trajectory pathways were multiplied with the regional primary $PM_{2.5}$ emission fluxes to quantify the contribution of regional transport of $PM_{2.5}$ to air quality change in the YRMB area with identifying the patterns of regional transport of $PM_{2.5}$ over CEC. The primary $PM_{2.5}$ emission data of year 2016 from the Multi-resolution Emission Inventory for China (MEIC, http://www.meicmodel.org/) were selected for use as the regional $PM_{2.5}$ emission fluxes in this study.

Based on the FLEXPART-WRF backward trajectory simulation, the upstream sources of $PM_{2.5}$ emissions for heavy air pollution in Wuhan could be identified. The contribution rates $\boldsymbol{rate_{i,j}}$ of regional transport of $PM_{2.5}$ from the upstream sources to air pollution in the downstream receptor region of YRMB were calculated by Eq.(1), and the total contribution $\boldsymbol{R}$ of regional transport from the non-local emission sources are estimated by Eq. (2) (Chen et al., 2017b; Ding et al., 2009).

$$rate_{i,j} = \frac{E_{i,j} \times r_{i,j}}{\sum_{1,1}^{N,S} E_{i,j} \times r_{i,j}} \qquad (1)$$

$$R = \sum_{(N_1,S_1)}^{(N_2,S_2)} rate_{i,j} \qquad (2)$$

where the subscripts $\boldsymbol{i}$ and **j** represent a grid location ($\boldsymbol{i, j}$) over the 48-hr backward trajectory from the first grid ($\boldsymbol{i}$=1, $\boldsymbol{j}$=1) in Wuhan (30.61°N, 114.42°E) to the last grid ($\boldsymbol{i}$=*N*, $\boldsymbol{j}$=*S*) over CEC; $\mathbf{r}_{i,j}$ represents the residence time of $PM_{2.5}$ particles simulated by FLEXPART-WRF; and $E_{i,j}$ represents the $PM_{2.5}$ emission flux over the grid. In Eq. (2), the first grid location (N_1, S_1) and the last grid location (N_2, S_2) over the non-local emission sources and the local area of Wuhan were determined respectively by the regional transport of $PM_{2.5}$ pathways and the YRMB area in Wuhan as simulated by FLEXPART-WRF.

3. Results and Discussion

3.1 Variations in local $PM_{2.5}$ concentrations in January 2016

Based on the National Ambient Air Quality Standards of China released by the Ministry of Ecology and Environment of China in 2012 (http://www.mee.gov.cn/), light and heavy air pollution levels of $PM_{2.5}$ are categorized by the daily average $PM_{2.5}$ concentrations exceeding 75 μg m^{-3} and 150 μg m^{-3} in ambient air, respectively. The daily variations of $PM_{2.5}$ concentrations over January 2016 averaged over ten observational sites in Wuhan are illustrated in Figure 3a. The average monthly $PM_{2.5}$ concentration reached 105.8μg m^{-3} in Wuhan, where the daily $PM_{2.5}$ concentrations exceeded 75 μg m^{-3} on 27 days during the entire month of January 2016 (Fig. 3a), indicating that this YRMB urban area was suffering under significant $PM_{2.5}$ pollution during this wintertime period. As shown in Figure 3a, a 21-day prolonged air pollution event resulted from high levels of daily $PM_{2.5}$ concentrations (>75 μg m^{-3}) over January 1 to 21, 2016. During this 21-day period of air pollution, three notably heavy air pollution events occurred on January 4, 10-12 and 18 with excessive daily $PM_{2.5}$ concentrations (>150 μg m^{-3}); these three events are marked as P1, P2 and P3 in Figure 3. Based on the observation in January 2016, we found the interesting phenomenon of an apparent about 7-day cycle of heavy air pollution in January 2016, reflecting an important modulation of meteorological oscillation in the East Asian winter monsoonal winds affecting air pollution over the YRMB region (Xu et al., 2016a). A period analysis on long-term observation data of air quality could provide the further understanding on air quality changes in associated with meteorological drivers.

Figure 3b presents the hourly changes of $PM_{2.5}$ concentrations during the three heavy air pollution events P1, P2 and P3. The heavy pollution event P1 on January 4 started at 11:00 a.m. (local time is used for all events) and ended at 11:00 p.m. at the same day with an observed $PM_{2.5}$ concentration peak of 471.1 μg m^{-3}. The event P2 occurred from 10:00 p.m. on January 10 to 00:00 a.m. on January 12 with a duration of 26 h with two peaks in $PM_{2.5}$ concentrations of 231.4 μg m^{-3} and 210.6 μg m^{-3}. The event P3 was observed between 7:00 p.m. on January 17 and 2:00

p.m. on January 18 with an explosive growth rate of 42.9 μg m^{-3} h^{-1} in $PM_{2.5}$ concentrations. Those three heavy $PM_{2.5}$ pollution episodes over the YRMB region were characterized by short durations of less than 26 h from rapid accumulation to fast dissipation.

The changes in $PM_{2.5}$ concentrations presented the less differences between the suburban and urban sites with the similar patterns and peaks of hourly changes during the heavy pollution periods with $PM_{2.5}$ concentrations exceeding 150 μg m^{-3} (Figs. S3, S4 and S5), demonstrating the regional heavy air pollution in a large area of the YRMB region with the contribution of regional transport over CEC, while the obvious differences in air pollutant concentrations were measured with the relative high and low concentrations of $PM_{2.5}$ respectively at urban sites and suburban site during the clean air periods with $PM_{2.5}$ concentrations below 75 μg m^{-3} in January 2016 (Figs. S3, S4 and S5), reflecting the important influence of high air pollutant emission over urban area on local air quality.

3.2 Meteorological influences on $PM_{2.5}$ changes in Wuhan

Using the environmental and meteorological data observed in Wuhan in January 2016, the effects of the meteorological conditions on $PM_{2.5}$ concentrations in the YRMB region were statistically analyzed in regards to hourly variations of surface $PM_{2.5}$ concentrations, near-surface wind speed (WS), wind direction (WD), surface air temperature (T), air pressure (P) and relative humidity (RH) (Fig. 4). Among the observed hourly changes in $PM_{2.5}$ concentrations and meteorological elements shown in Figure 4, the changes of $PM_{2.5}$ concentrations were found respectively with the obviously positive correlations to surface air temperature and relative humidity, as well as a pronounced negative correlation to surface air pressure and a weak positive correlation to near-surface wind speed in January 2016 (Table 1). There are several reasons associated with this result. Firstly, the lower near-surface wind speed could alter the concentrations of air pollutants with a weaker advection of cold air, in conjunction with strong subsidence and stable atmospheric stratification, easily producing a stagnation area in the lower troposphere with resulting in regional pollutant accumulations for the development of haze events. Secondly, in the presence of high soil moisture, strong surface evaporation could increase the near-surface relative humidity, which is also conducive to hygroscopic growth of participles for haze formation (Dawson et al., 2014; Xu et al., 2016a). High air temperature and strong solar radiation could enhance chemical conversions for the formation of secondary aerosols in the atmosphere (He et al., 2012; Huang et al., 2014). Furthermore, precipitation could impact the emissions, and depositions of air pollutants (Dawson et al., 2007; Cheng et al., 2016). These air pollutant and meteorological observations could reflect the special influences of meteorological factors (winds, air temperature, humidity, precipitation etc.) on physical and chemical processes in the ambient atmosphere, affecting air quality change in the YRMB region.

When we focused on the meteorological changes leading to high $PM_{2.5}$ levels exceeding 150 μg m^{-3} during these heavy air pollution events, it is noteworthy that all three heavy pollution episodes P1, P2 and P3 were accompanied with strong near-surface wind speeds in the northerly direction, as well as evident turning points in prevailing conditions leading to falling surface air temperatures and increasing surface air pressure (noted as a rectangle with red dashed lines in Fig. 4). The conditions observed during these three heavy pollution episodes present the typical meteorological characteristics of cold air invasion over the East Asian monsoon region. The southward advance of a cold front could drive the regional transport of air pollutants over CEC

(Kang et al., 2019). Climatologically, a strong northerly wind, low air temperature and high air pressure are typical features of an incursion of cold air during East Asian winter monsoon season in CEC, which could disperse air pollutants for improving air quality in the NCP region (Miao et al., 2018; Xu et al., 2016b). Differing to the meteorological conditions of stagnation with weak winds observed for heavy air pollution events in the major air pollution regions of CEC (Ding et al., 2017;Huang et al., 2018), the meteorological conditions with strong near-surface wind were anomalously accompanied with the intensification of $PM_{2.5}$ during heavy air pollution periods over the study area in the YRMB in January 2016 (Fig.4). This could imply an importance of regional air pollutant transport in worsening air quality over the YRMB, driven by the strong northerly winds during the season of East Asian winter monsoon.

3.3 A unique meteorological condition of "non-stagnation" for heavy $PM_{2.5}$ pollution

To further investigate the connection of meteorological elements in the near-surface layer with changes in air quality affected by $PM_{2.5}$ concentrations in the YRMB region, we carried out a more detailed correlation analysis of $PM_{2.5}$ concentrations in Wuhan with near-surface wind speed and air temperature for three different levels of $PM_{2.5}$ concentrations: clean air environment ($PM_{2.5}$<75 μg m^{-3}), light air pollution (75 μg m^{-3} ≤ $PM_{2.5}$ <150 μg m^{-3}) and heavy air pollution ($PM_{2.5}$ ≥150 μg m^{-3}) periods (Table 2). As seen in Table 2, the surface $PM_{2.5}$ concentrations were positively correlated with air temperature, as well as negatively correlated with wind speeds during the periods of clean air environment and light air pollution. It should be emphasized here that a significantly negative correlation (R=-0.19) of $PM_{2.5}$ concentrations with near-surface wind speed for the light air pollution period could indicate that weak winds are favorable for local $PM_{2.5}$

accumulation, reflecting an important effect of local air pollutant emissions on light air pollution periods over the YRMB area. In January 2016, the overall wind speed of Wuhan was weak with a monthly mean value of 2.0 m s^{-1}, which could prove beneficial to maintaining the high $PM_{2.5}$ levels in the prolonged air pollution events experienced in the YRMB area. However, a significantly positive correlation (R=0.41) existed between heavy air pollution levels of $PM_{2.5}$ concentrations ($PM_{2.5}$ >150 μg m^{-3}) and strong near-surface wind speeds during the heavy air pollution periods, which was inconsistent with the meteorological conditions of stagnation observed in the near-surface layer with weak winds associated with heavy air pollution in East China (Cao et al., 2012; Deng et al., 2011). The meteorology and environment conditions in the YRMB region indicate the close association of heavy air pollution periods enhancing $PM_{2.5}$ concentrations with strong winds (Fig. 4, Table 2), reflecting a key role of regional transport of air pollutants in the development of the YRMB's heavy air pollution periods.

In order to clearly illustrate the impact of wind speed and direction on the $PM_{2.5}$ concentrations associated with the regional transport of upwind air pollutants, Figure 5 presents the relation of hourly changes in surface $PM_{2.5}$ concentrations (in color contours) to near-surface wind speed (in radius of round) and direction (in angles of round) in Wuhan during January 2016. As can be seen in Figure 5, strong northerly winds accompanied extremely high $PM_{2.5}$ concentrations (>150 μg m^{-3}) during heavy air pollution periods, including the northeast gale exceeding 5 m s^{-1} during the extreme heavy pollution periods with extremely high $PM_{2.5}$ concentrations (>300 μg m^{-3}) over the YRMB region. These results reveal a unique meteorological condition of "non-stagnation" with strong winds during events of heavy air pollution over YRMB area. Conversely, the observed $PM_{2.5}$ concentrations ranging between 75 and 150 μg m^{-3} for light air pollution periods generally corresponded with low wind speed (<2 m s^{-1}) in the YRMB region (Fig. 5). Therefore, it is the meteorological condition for stagnation characterized by weak winds involved in the accumulation of local air pollutants that is responsible for the light air pollution periods of YRMB. Meteorological impacts on air quality could include not only the stagnant condition of meteorology with weak winds and stable boundary layer, but also air temperature, humidity, precipitation, atmospheric radiation etc. in close connection with atmospheric physical and chemical processes. The meteorological drivers of air quality change are complicated by a series of physical and chemical processes in the atmosphere especially the formation of secondary air pollutants with strong hygroscopic growth in the humid air environment overlying the dense water network (see Fig. 1b) in the YRMB region (Cheng et al., 2014; He et al., 2012; Huang et al., 2014).

As shown in Figure 3a, the heavy pollution periods with the daily average $PM_{2.5}$ concentrations exceeding 150 μg m^{-3} in ambient air, respectively occurred on January 4, 10-12 and 18, and the clean air periods with the daily average $PM_{2.5}$ concentrations below 75 μg m^{-3} happening on January 22 and 24-27, 2016. The air sounding data observed in Wuhan were used to compare the structures of atmospheric boundary layer during the heavy air pollution and clean air periods. Figure 6 presents the vertical profiles of air temperature, wind velocity and potential temperature averaged for the heavy $PM_{2.5}$ pollution and clean air periods in January 2016. It can be clearly seen that the inversion layer of air temperature did not exist during the heavy pollution periods, while a near-surface inversion layer appeared at the height of about 200 m during the clean air periods (Fig. 6a). Compared to the clean air period, the heavy air pollution events had stronger winds within the 1000-m layer but weaker winds above the 1000 m layer (Fig. 6b), indicating that regional transport of $PM_{2.5}$ was mainly limited to the 1000m layer, especially between 250 m and 800 m. These vertical structures of horizontal wind could conduce the downward mixing of the regionally transported air pollutants and produce the near-surface accumulations of air pollutants over the YRMB area with elevated ambient $PM_{2.5}$ concentrations, thus contributing to a heavy air pollution.

To quantitatively characterize the stability of the atmospheric boundary layer, the vertical profiles of potential air temperature (θ) were calculated with air temperature and pressure (Fig. 6c). The vertical change rate of θ was used to quantify the static stability of the boundary layer in this study (Oke, 2002). A lower vertical change rate of θ generally indicates a decreasing stability or increasing instability of the boundary layer. The averaged static stability values of the near-surface layer below a height of 200 m during the heavy pollution and clean air periods were approximately 4.4 K km^{-1} and 13.2 K km^{-1}, respectively (Table 3). This obvious decrease in stability of the boundary layer from clean air to heavy pollution periods indicates an anomalous tendency of the unstable boundary layer for the heavy pollution periods during January 2016 in the YRMB area.

The meteorological conditions of stagnation characterized by weak wind, temperature inversion and a stable vertical structure of the atmospheric boundary layer is generally accepted as the typical meteorological drivers for heavy air pollution (An et al., 2019; Ding et al., 2017). Nevertheless, this study of environmental and meteorological observations in the YRMB region revealed a unique meteorological condition of "non-stagnation" in the atmospheric boundary layer during heavy air pollution periods characterized by strong wind, lack of an inversion layer and a more unstable structure of the atmospheric boundary layer. These "non-stagnant" meteorological conditions could be generally regarded as the typical pattern of atmospheric circulation that facilitates the regional transport of air pollutants from upstream source to downwind receptor regions. Regional transport of $PM_{2.5}$ connected with the source-receptor relationship between the air pollution regions in CEC and the YRMB area was further investigated based on the following observational and modeling analyses.

3.4 Changes of $PM_{2.5}$ and winds observed over CEC

The monthly averages of $PM_{2.5}$ concentrations and the anomalies of wind speed averaged in three heavy air pollution periods relative to the monthly mean wind speed in January 2016 observed over CEC are exhibited in Figure 7. In January 2016, a large area of CEC experienced air pollution with the high levels of $PM_{2.5}$ >75 μg m^{-3} especially severe in the NCP region and the Fenhe-Weihe Plain in Central China (Fig. 7a). As seen in Figure 7, Wuhan (site 1 in Fig. 7a) and the surrounding YRMB region were situated in the downwind southern edge of air pollution area blanketing the CEC region (Fig. 7a), where the northerly winds prevailed in January 2016 (Fig. 7b). Climatologically, CEC is a typical region of East Asian monsoons dominated with wintertime northerlies (Ding, 1993). It is notable that the anomalously stronger northerly winds were observed over the upstream CEC regions during three periods of wintertime heavy $PM_{2.5}$ pollution in the downwind YRMB region (Fig. 7b). Driven by the stronger northerly winds, the regional transport of air pollutants from the source regions in windward CEC could largely contribute to heavy air pollution in the downwind receptor region of YRMB.

In order to explore the connection of regional transport of $PM_{2.5}$ over CEC to three events of heavy air pollution in the YRMB region, six observational sites were selected from the northwestern, northern and northeastern directions over the upstream CEC region (Fig. 7a) to represent three different routes of regional transport of $PM_{2.5}$ to Wuhan (site 1 in Fig. 7a) in the YRMB, governed with the southward incursion of stronger northerly winds (Fig. 7b). Figure 8 presents the the temporal changes of $PM_{2.5}$ concentrations and wind speed along three typical routes of regional transport of $PM_{2.5}$ over CEC. The southeastward movement of heavy $PM_{2.5}$ pollution driven by stronger northerly winds from Luoyang and Xinyang to Wuhan (sites 3, 2, and 1 in Fig. 7) presents a northwestern route of regional transport of $PM_{2.5}$ for the heavy air pollution period P1 in the YRMB area (see upper panels of Fig. 8). The westward advance of $PM_{2.5}$ peaks governed by northeastern winds from Tongling and Hefei to Wuhan (sites 6, 5, and 1 in Fig. 7a). Regional transport of $PM_{2.5}$ across Eastern China to the YRMB in Central China exerted a significant impact on the heavy air pollution period P2 (see middle panels of Fig. 8). A northern pathway of regional transport of $PM_{2.5}$ connected Zhengzhou and Xinyang to Wuhan (sites 4, 2, and 1 in Fig. 7a) during the YRMB's heavy air pollution period P3 with anomalously strong northerly winds (see Fig. 7b and lower panels of Fig. 8). It is noteworthy in Figure 8 that the heavy $PM_{2.5}$ pollution periods at the upstream sites Hefei, Tongling, Luoyang, Xinyang and Zhengzhou (sites 2-6 in Fig. 7a) were generally dispelled by strong northerly winds, while strong northerly winds could trigger the periods of heavy $PM_{2.5}$ pollution in the YRMB region (Wuhan, site 1 in Fig. 7a), and such inverse effects of strong winds on heavy air pollution in the CEC and YRMB regions reflect an important role of regional transport of air pollutants in cleaning and worsening air pollution respectively in the upstream CEC source regions and the downstream YRMB receptor region.

The regional transport over CEC associated with the source-receptor relationship directing heavy $PM_{2.5}$ pollution to the YRMB region was revealed with observational analysis. The FLEXPART-WRF backward trajectory modeling was used to further identify the patterns of regional transport of $PM_{2.5}$ and estimate the resulting contribution to heavy air pollution in the YRMB region in the following Sect.

3.5 Contribution of regional transport of $PM_{2.5}$ to heavy pollution

In this study for the receptor of Wuhan, the $PM_{2.5}$ contributions of regional transport over CEC to air pollution in the downwind receptor region could be approximately estimated based on the product of the residence time of air particles during regional transport simulated by FLEXPART-WRF and the $PM_{2.5}$ emission flux over the source grid in CEC with Eq. (1), yielding a so-called potential source contribution map, which is the geographical distribution of the regional transport contribution rates (%) of the emission source grid cell to $PM_{2.5}$ pollution at the receptor of Wuhan (Fig. 9).

The non-local emission sources that affected $PM_{2.5}$ concentrations during three heavy pollution periods through regional transport to the YRMB area were quantified over CEC by using the $PM_{2.5}$ contribution rates calculated with Eq. (1). Combining the distribution of high $PM_{2.5}$ contribution rates with the prevailing winds experienced during the three heavy $PM_{2.5}$ pollution periods, the major pathways of regional transport of $PM_{2.5}$ over CEC could be recognized as shown in Figure 9. During the heavy air pollution period P1 in the YRMB region, the regional transport of air pollutants was centered along a northwestern route from the Fenhe-Weihe Plain in Central China and a northeastern route from the YRD region in Eastern China (Fig. 9a). The YRD emission sources of air pollutants in Eastern China exerted a large impact on the heavy air pollution period P2 through regional transport of $PM_{2.5}$ cross Eastern China to the YRMB region along the north side of Yangtze River (Fig. 9b). Two major regional transport pathways of $PM_{2.5}$ indicated by the spatial distribution of high contribution rates of $PM_{2.5}$ from the NCP and YRD regions respectively to the elevated $PM_{2.5}$ concentrations during the YRMB's heavy air pollution period P3 (Fig. 9c). Governed by the anomalous northerly winds in January 2016 (Fig. 7b), the regional transport of $PM_{2.5}$ from the air pollutant emission source regions in CEC provided a significant contribution to the wintertime heavy $PM_{2.5}$ pollution observed in the YRMB region (Figs. 7-9), which was confirmed by the results of the FLEXPART-WRF backward trajectory simulation utilized in this study.

The $PM_{2.5}$ contributions of regional transport over CEC to $PM_{2.5}$ concentrations during three heavy $PM_{2.5}$ pollution periods P1, P2 and P3 in the YRMB area were estimated using Eq. (2) with resulting high contribution rates of 68.1%, 60.9% and 65.3%, respectively (Table 4). The regional transport of $PM_{2.5}$ from non-local air pollutant emissions could contribute more than 65% of the $PM_{2.5}$ concentrations to the heavy air pollution in the YRMB region during the study period, revealing the large contribution of regional transport of $PM_{2.5}$ over CEC to the enhancement of $PM_{2.5}$ levels in the YRMB area for the wintertime heavy air pollution.

It should be pointed out that the potential source contribution is estimated based on transport alone, ignoring chemical and removal processes. We also understand that the physical and chemical processes such as complex deposition and chemical conversion for the formation of secondary particles are not introduced in the FLEXPART-WRF emulation, which could represent the basic features of contribution and patterns of regional $PM_{2.5}$ transport over CEC, when limited to the primary $PM_{2.5}$ particles highlighted in this study.

Normally people rely on 3-D numerical models with process analysis capability such as integrated process rates (IPRs) to quantify the contributions of regional transport to the occurrence of air pollution episodes. The simulations with a Lagrange particle dispersion model FLEXPART-WRF are utilized to calculate the percentage contribution of regional transport with identifying the transport pathway in this study. The major uncertainty of this method for such calculation as compared to other methods like IPRs is that the physical and chemical processes such as chemical conversion for the formation of secondary particles are not introduced in the FLEXPART-WRF simulation, Considering less precipitation in the winter monsoon season over CEC, how this methodology with FLEXPART-WRF mideling is proven robustness to quantify the regional transport contribution with the uncertainty range here could mostly rely on a portion of secondary organic and inorganic aerosols, which are resulted from the complex physical and chemical processes in the atmosphere.

4. Conclusions

This study investigated the ambient $PM_{2.5}$ variations over Wuhan, a typical YRMB area in Central China in January 2016 through analysis of observational data of environment and meteorology, as well as via FLEXPART-WRF simulation to explore 1) the meteorological processes involved in the regional transport of air pollutants and 2) regional transport patterns of $PM_{2.5}$ with the contribution to heavy air pollution in the YRMB region. Based on observation and simulation studies on the meteorological conditions of air pollution in January 2016 over the YRMB region, we found the unique "non-stagnant" atmospheric boundary layer for wintertime heavy air pollution in the YRMB area aggravated by regional transport of $PM_{2.5}$ over CEC, which facilitates understanding of the air pollutant source-receptor relationship of regional transport in air quality change.

The effects of meteorology and regional transport of $PM_{2.5}$ on air qaulity change were focused on three heavy $PM_{2.5}$ pollution periods in January 2016. This study of environmental and meteorological observations in the YRMB region revealed a unique “non-stagnant” meteorological condition of the boundary layer characterized by strong wind, no inversion layer and a more unstable structure in the atmospheric boundary layer associated with heavy air pollution periods with high $PM_{2.5}$ concentrations in the YRMB region, The study represents a great interest to air quality community given the unique features of air pollution meteorology which are very different from those “stagnant” meteorological conditions presented in the textbooks.

Although the emissions and local accumulation of air pollutants in the YRMB area could lead to the formation of light air pollution, in regards to $PM_{2.5}$, over the YRMB region, the regional transport of $PM_{2.5}$ from upstream source regions of air pollutant emissions in CEC contributed significantly to 65% of the exceedances of $PM_{2.5}$ concentrations during wintertime heavy air pollution in the downwind YRMB region in January 2016, as governed by the strong northerly winds in the East Asian winter monsoon season over CEC.

Based on the variations of air quality and meteorology in a typical urban YRMB region in January 2016, this study revealed a unique “non-stagnant” meteorological condition for heavy air pollution in the YRMB region with strong contribution of regional transport of $PM_{2.5}$ over China. These conditions and contributions can be investigated further with climate analyses of long-term observations and a more comprehensive modeling of air quality and meteorology.

Data availability: Data used in this paper can be provided by Chao Yu (ychao012@foxmail.com) upon request.

Supplement: The supplement related to this article is available on┐line at: https://doi.org/

Author contributions: CY, TZ and YB conducted the study design. XY, LZ and SK provided the observational data. LZ assisted with data processing. CY wrote the manuscript with the help of TZ and XY. YB, SK, JH, CC, JY, YY, GM, MW and JC were involved in the scientific interpretation and discussion. All of the authors provided commentary on the paper.

Competing interests: The authors declare that they have no conflicts of interest.

Acknowledgement: This study was jointly funded by the National Natural Science Foundation of China (41830965; 91744209), the National Key R & D Program Pilot Projects of China (2016YFC0203304) and the Postgraduate Research & Practice Innovation Program of Jiangsu Province (KYCX18_1027).

References

Acciai, C., Zhang, Z., Wang, F., Zhong, Z., and Lonati, G.: Characteristics and source Analysis of trace Elements in $PM_{2.5}$ in the Urban Atmosphere of Wuhan in Spring, Aerosol and Air Quality Research, 17, 2224-2234, https://doi.org/10.4209/aaqr.2017.06.0207, 2017.

An, X., Yao, B., Li, Y., Li, N., and Zhou, L.: Tracking source area of Shangdianzi station using Lagrangian particle dispersion model of FLEXPART, Meteorological Applications, 21, 466-473, https://doi.org/10.1002/met.1358, 2014.

An, Z., Huang, R. J., Zhang, R., Tie, X., Li, G., Cao, J., Zhou, W., Shi, Z., Han, Y., Gu, Z., and Ji, Y.: Severe haze in northern China: A synergy of anthropogenic emissions and atmospheric processes, Proceedings of the National Academy of Sciences, 116, 8657-8666, https://doi.org/10.1073/pnas.1900125116, 2019.

Brioude, J., Arnold, D., Stohl, A., Cassiani, M., Morton, D., Seibert, P., Angevine, W., Evan, S., Dingwell, A., Fast, J. D., Easter, R. C., Pisso, I., Burkhart, J., and Wotawa, G.: The Lagrangian particle dispersion model FLEXPART-WRF version 3.1, Geoscientific Model Development, 6, 1889-1904, https://doi.org/10.5194/gmd-6-1889-2013, 2013.

Cao, J.-j., Wang, Q.-y., Chow, J. C., Watson, J. G., Tie, X.-x., Shen, Z.-x., Wang, P., and An, Z.-s.: Impacts of aerosol compositions on visibility impairment in Xi'an, China, Atmospheric Environment, 59, 559-566, https://doi.org/10.1016/j.atmosenv.2012.05.036, 2012.

Chang, X., Wang, S., Zhao, B., Cai, S., and Hao, J.: Assessment of inter-city transport of particulate matter in the Beijing-Tianjin-Hebei region, Atmospheric Chemistry and Physics, 18, 4843-4858, https://doi.org/10.5194/acp-18-4843-2018, 2018.

Chen, B., Xu, X.-D., and Zhao, T.: Quantifying oceanic moisture exports to mainland China in association with summer precipitation, Climate Dynamics, 51, 4271-4286, https://doi.org/10.1007/s00382-017-3925-1, 2017a.

Chen, S., Zhou, G., and Zhu, B.: A method for fast quantification of air pollutant sources（in Chinese）, Acta Scientiae Circumstantiae, 37, 2474-2481, https://doi.org/10.13671/j.hjkxxb.2017.0045, 2017b.

Cheng, H., Gong, W., Wang, Z., Zhang, F., Wang, X., Lv, X., Liu, J., Fu, X., and Zhang, G.: Ionic composition of submicron particles ($PM_{1.0}$) during the long-lasting haze period in January 2013 in Wuhan, central China, Journal of Environmental Sciences, 26, 810-817, https://doi.org/10.1016/s1001-0742(13)60503-3, 2014.

Cheng, X., Zhao, T., Gong, S., Xu, X., Han, Y., Yin, Y., Tang, L., He, H., and He, J.: Implications of East Asian summer and winter monsoons for interannual aerosol variations over central-eastern China, Atmospheric Environment, 129, 218-228, https://doi.org/10.1016/j.atmosenv.2016.01.037, 2016.

Cheng, Y. F., Wiedensohler, A., Eichler, H., Heintzenberg, J., Tesche, M., Ansmann, A., Wendisch, M., Su, H., Althausen, D., and Herrmann, H.: Relative humidity dependence of aerosol optical properties and direct radiative forcing in the surface boundary layer at Xinken in Pearl River Delta of China: An observation based numerical study, Atmospheric Environment, 42, 6373-6397, https://doi.org/10.1016/j.atmosenv.2008.04.009, 2008.

Dawson, J., Adams, P., and Pandis, S.: Sensitivity of $PM_{2.5}$ to climate in the Eastern US: a modeling case study, Atmospheric chemistry and physics, 7, 4295-4309, https://doi.org/10.5194/acp-7-4295-2007, 2007.

Dawson, J. P., Bloomer, B. J., Winner, D. A., and Weaver, C. P.: Understanding the Meteorological Drivers of U.S. Particulate Matter Concentrations in a Changing Climate, Bulletin of the American Meteorological Society, 95, 521-532, https://doi.org/10.1175/bams-d-12-00181.1, 2014.

De Foy, B., Burton, S. P., Ferrare, R. A., Hostetler, C. A., Hair, J. W., Wiedinmyer, C., and Molina, L. T.: Aerosol plume transport and transformation in high spectral resolution lidar measurements and WRF-Flexpart simulations during the MILAGRO Field Campaign, Atmospheric Chemistry and Physics, 11, 3543-3563, https://doi.org/10.5194/acp-11-3543-2011, 2011.

Deng, J., Wang, T., Jiang, Z., Xie, M., Zhang, R., Huang, X., and Zhu, J.: Characterization of visibility and its affecting factors over Nanjing, China, Atmospheric Research, 101, 681-691, https://doi.org/10.1016/j.atmosres.2011.04.016, 2011.

Ding, A., Wang, T., Xue, L., Gao, J., Stohl, A., Lei, H., Jin, D., Ren, Y., Wang, X., and Wei, X.: Transport of north China air pollution by midlatitude cyclones: Case study of aircraft measurements in summer 2007, Journal of Geophysical Research: Atmospheres, 114, https://doi.org/doi:10.1029/2008JD011023, 2009.

Ding, Y.: Monsoons over china, Springer Science & Business Media, 1993.

Ding, Y., Wu, P., Liu, Y., and Song, Y.: Environmental and Dynamic Conditions for the Occurrence of Persistent Haze Events in North China, Engineering, 3, 266-271, https://doi.org/10.1016/j.eng.2017.01.009, 2017.

Fast, J. D., and Easter, R. C.: A Lagrangian particle dispersion model compatible with WRF, 7th WRF Users Workshop, NCAR, 2006, 19-22.

Fuzzi, S., Baltensperger, U., Carslaw, K., Decesari, S., Denier van der Gon, H., Facchini, M. C., Fowler, D., Koren, I., Langford, B., Lohmann, U., Nemitz, E., Pandis, S., Riipinen, I., Rudich, Y., Schaap, M., Slowik, J. G., Spracklen, D. V., Vignati, E., Wild, M., Williams, M., and Gilardoni, S.: Particulate matter, air quality and climate: lessons learned and future needs, Atmospheric Chemistry and Physics, 15, 8217-8299, https://doi.org/10.5194/acp-15-8217-2015, 2015.

Gong, W., Zhang, T., Zhu, Z., Ma, Y., Ma, X., and Wang, W.: Characteristics of $PM_{1.0}$, $PM_{2.5}$, and PM_{10}, and Their Relation to Black Carbon in Wuhan, Central China, Atmosphere, 6, 1377-1387, https://doi.org/10.3390/atmos6091377, 2015.

Grell, G. A., Peckham, S. E., Schmitz, R., McKeen, S. A., Frost, G., Skamarock, W. C., and Eder, B.: Fully coupled "online" chemistry within the WRF model, Atmospheric Environment, 39, 6957-6975, https://doi.org/10.1016/j.atmosenv.2005.04.027, 2005.

He, J., Mao, H., Gong, S., Yu, Y., Wu, L., Liu, H., Chen, Y., Jing, B., Ren, P., and Zou, C.: Investigation of Particulate Matter Regional Transport in Beijing Based on Numerical Simulation, Aerosol and Air Quality Research, 17, 1181-1189, https://doi.org/10.4209/aaqr.2016.03.0110, 2017.

He, K., Zhao, Q., Ma, Y., Duan, F., Yang, F., Shi, Z., and Chen, G.: Spatial and seasonal variability of $PM_{2.5}$ acidity at two Chinese megacities: insights into the formation of secondary inorganic aerosols, Atmospheric Chemistry and Physics, 12, 1377-1395, https://doi.org/10.5194/acp-12-1377-2012, 2012.

Hong, S.-Y., Noh, Y., and Dudhia, J.: A new vertical diffusion package with an explicit treatment of entrainment processes, Monthly weather review, 134, 2318-2341, https://doi.org/10.1175/MWR3199.1,2006, 2006.

Hu, J., Li, Y., Zhao, T., Liu, J., Hu, X.-M., Liu, D., Jiang, Y., Xu, J., and Chang, L.: An important mechanism of regional O_3 transport for summer smog over the Yangtze River Delta in eastern China, Atmospheric Chemistry and Physics, 18, 16239-16251, https://doi.org/10.5194/acp-18-16239-2018, 2018.

Huang, Q., Cai, X., Wang, J., Song, Y., and Zhu, T.: Climatological study of the Boundary-layer air Stagnation Index for China and its relationship with air pollution, Atmospheric Chemistry and Physics, 18, 7573-7593, https://doi.org/10.5194/acp-18-7573-2018, 2018.

Huang, R. J., Zhang, Y., Bozzetti, C., Ho, K. F., Cao, J. J., Han, Y., Daellenbach, K. R., Slowik, J. G., Platt, S. M., Canonaco, F., Zotter, P., Wolf, R., Pieber, S. M., Bruns, E. A., Crippa, M., Ciarelli, G., Piazzalunga, A., Schwikowski, M., Abbaszade, G., Schnelle-Kreis, J., Zimmermann, R., An, Z., Szidat, S., Baltensperger, U., El Haddad, I., and Prevot, A. S.: High secondary aerosol contribution to particulate pollution during haze events in China, Nature, 514, 218-222, https://doi.org/10.1038/nature13774, 2014.

Jiang, C., Wang, H., Zhao, T., Li, T., and Che, H.: Modeling study of $PM_{2.5}$ pollutant transport across cities in China's Jing-Jin-Ji region during a severe haze episode in December 2013, Atmospheric Chemistry and Physics, 15, 5803-5814, https://doi.org/10.5194/acp-15-5803-2015, 2015.

Kang, H., Zhu, B., Gao, J., He, Y., Wang, H., Su, J., Pan, C., Zhu, T., and Yu, B.: Potential impacts of cold frontal passage on air quality over the Yangtze River Delta, China, Atmospheric Chemistry and Physics, 19, 3673-3685, https://doi.org/10.5194/acp-19-3673-2019, 2019.

Miao, Y., Guo, J., Liu, S., Zhao, C., Li, X., Zhang, G., Wei, W., and Ma, Y.: Impacts of synoptic condition and planetary boundary layer structure on the trans-boundary aerosol transport from Beijing-Tianjin-Hebei region to northeast China, Atmospheric Environment, 181, 1-11, https://doi.org/10.1016/j.atmosenv.2018.03.005, 2018.

Mlawer, E. J., Taubman, S. J., Brown, P. D., Iacono, M. J., and Clough, S. A.: Radiative transfer for inhomogeneous atmospheres: RRTM, a validated correlated-k model for the longwave, Journal of Geophysical Research: Atmospheres, 102, 16663-16682, https://doi.org/10.1029/97jd00237, 1997.

Morrison, H., Thompson, G., and Tatarskii, V.: Impact of Cloud Microphysics on the Development of Trailing Stratiform Precipitation in a Simulated Squall Line: Comparison of One- and Two-Moment Schemes, Monthly Weather Review, 137, 991-1007, https://doi.org/10.1175/2008mwr2556.1, 2009.

Nel, A.: Air pollution-related illness: effects of particles, Science, 308, 804-806, https://doi.org/10.1126/science.1108752, 2005.

Oke, T. R.: Boundary layer climates, Routledge, 2002.

Qiao, X., Guo, H., Tang, Y., Wang, P., Deng, W., Zhao, X., Hu, J., Ying, Q., and Zhang, H.: Local and regional contributions to fine particulate matter in the 18 cities of Sichuan Basin, southwestern China, Atmospheric Chemistry and Physics, 19, 5791-5803, https://doi.org/10.5194/acp-19-5791-2019, 2019.

Sauvage, B., Fontaine, A., Eckhardt, S., Auby, A., Boulanger, D., Petetin, H., Paugam, R., Athier, G., Cousin, J.-M., Darras, S., Nédélec, P., Stohl, A., Turquety, S., Cammas, J.-P., and Thouret, V.: Source attribution using FLEXPART and carbon monoxide emission inventories: SOFT-IO version 1.0, Atmospheric Chemistry and Physics, 17, 15271-15292, https://doi.org/10.5194/acp-17-15271-2017, 2017.

Seibert, P., and Frank, A.: Source-receptor matrix calculation with a Lagrangian particle dispersion model in backward mode, Atmospheric Chemistry and Physics, 4, 51-63, https://doi.org/10.5194/acp-4-51-2004, 2004.

Stohl, A., Forster, C., Eckhardt, S., Spichtinger, N., Huntrieser, H., Heland, J., Schlager, H., Wilhelm, S., Arnold, F., and Cooper, O.: A backward modeling study of intercontinental pollution transport using aircraft measurements, Journal of Geophysical Research: Atmospheres, 108, https://doi.org/10.1029/2002jd002862, 2003.

Stohl, A., Forster, C., Frank, A., Seibert, P., and Wotawa, G.: Technical note: The Lagrangian particle dispersion model FLEXPART version 6.2, Atmospheric Chemistry & Physics, 5, 2461-2474, https://doi.org/10.5194/acp-5-2461-2005, 2005.

Taylor, K. E.: Summarizing multiple aspects of model performance in a single diagram, Journal of Geophysical Research: Atmospheres, 106, 7183-7192, https://doi.org/10.1029/2000jd900719, 2001.

Tie, X., Huang, R. J., Cao, J., Zhang, Q., Cheng, Y., Su, H., Chang, D., Poschl, U., Hoffmann, T., Dusek, U., Li, G., Worsnop, D. R., and O'Dowd, C. D.: Severe Pollution in China Amplified by Atmospheric Moisture, Science Report, 7, 15760, https://doi.org/10.1038/s41598-017-15909-1, 2017.

Voulgarakis, A., Savage, N., Wild, O., Braesicke, P., Young, P., Carver, G., and Pyle, J.: Interannual variability of tropospheric composition: the influence of changes in emissions, meteorology and clouds, Atmospheric Chemistry and Physics, 10, 2491-2506, https://doi.org/10.5194/acp-10-2491-2010, 2010.

Wang, H. L., Qiao, L. P., Lou, S. R., Zhou, M., Ding, A. J., Huang, H. Y., Chen, J. M., Wang, Q., Tao, S. K., Chen, C. H., Li, L., and Huang, C.: Chemical composition of $PM_{2.5}$ and meteorological impact among three years in urban Shanghai, China, Journal of Cleaner Production, 112, 1302-1311, https://doi.org/10.1016/j.jclepro.2015.04.099, 2016.

Wang, S. X., Zhao, B., Cai, S. Y., Klimont, Z., Nielsen, C. P., Morikawa, T., Woo, J. H., Kim, Y., Fu, X., Xu, J. Y., Hao, J. M., and He, K. B.: Emission trends and mitigation options for air pollutants in East Asia, Atmospheric Chemistry and Physics, 14, 6571-6603, https://doi.org/10.5194/acp-14-6571-2014, 2014.

Wu, J., Kong, S., Wu, F., Cheng, Y., Zheng, S., Yan, Q., Zheng, H., Yang, G., Zheng, M., Liu, D., Zhao, D., and Qi, S.: Estimating the open biomass burning emissions in central and eastern China from 2003 to 2015 based on satellite observation, Atmospheric Chemistry and Physics, 18, 11623-11646, https://doi.org/10.5194/acp-18-11623-2018, 2018.

Xu, G., Jiao, L., Zhang, B., Zhao, S., Yuan, M., Gu, Y., Liu, J., and Tang, X.: Spatial and Temporal Variability of the $PM_{2.5}/PM_{10}$ Ratio in Wuhan, Central China, Aerosol and Air Quality Research, 17, 741-751, https://doi.org/10.4209/aaqr.2016.09.0406, 2017.

Xu, J., Chang, L., Qu, Y., Yan, F., Wang, F., and Fu, Q.: The meteorological modulation on $PM_{2.5}$ interannual oscillation during 2013 to 2015 in Shanghai, China, Science of the Total Environment, 572, 1138-1149, https://doi.org/10.1016/j.scitotenv.2016.08.024, 2016a.

Xu, X., Zhao, T., Liu, F., Gong, S. L., Kristovich, D., Lu, C., Guo, Y., Cheng, X., Wang, Y., and Ding, G.: Climate modulation of the Tibetan Plateau on haze in China, Atmospheric Chemistry and Physics, 16, 1365-1375, https://doi.org/10.5194/acp-16-1365-2016, 2016b.

Zhai, S., An, X., Liu, Z., Sun, Z., and Hou, Q.: Model assessment of atmospheric pollution control schemes for critical emission regions, Atmospheric Environment, 124, 367-377, https://doi.org/10.1016/j.atmosenv.2015.08.093, 2016.

Zhang, F., Wang, Z. W., Cheng, H. R., Lv, X. P., Gong, W., Wang, X. M., and Zhang, G.: Seasonal variations and chemical characteristics of $PM_{2.5}$ in Wuhan, central China, Science of the Total Environment, 518-519, 97-105, https://doi.org/10.1016/j.scitotenv.2015.02.054, 2015.

Zhang, R., Li, Q., and Zhang, R.: Meteorological conditions for the persistent severe fog and haze event over eastern China in January 2013, Science China Earth Sciences, 57, 26-35, https://doi.org/10.1007/s11430-013-4774-3, 2013.

Zhang, X. Y., Wang, Y. Q., Niu, T., Zhang, X. C., Gong, S. L., Zhang, Y. M., and Sun, J. Y.: Atmospheric aerosol compositions in China: spatial/temporal variability, chemical signature, regional haze distribution and comparisons with global aerosols, Atmospheric Chemistry and Physics, 12, 779-799, https://doi.org/10.5194/acp-12-779-2012, 2012.

Zhao, T., Gong, S., Huang, P., and Lavoué, D.: Hemispheric transport and influence of meteorology on global aerosol climatology, Atmospheric Chemistry & Physics Discussions, 12, https://doi.org/10.5194/acp-12-7609-2012, 2012.

Zhao, X. J., Zhao, P. S., Xu, J., Meng, W., Pu, W. W., Dong, F., He, D., and Shi, Q. F.: Analysis of a winter regional haze event and its formation mechanism in the North China Plain, Atmospheric Chemistry and Physics, 13, 5685-5696, https://doi.org/10.5194/acp-13-5685-2013, 2013.

Zheng, H., Kong, S., Wu, F., Cheng, Y., Niu, Z., Zheng, S., Yang, G., Yao, L., Yan, Q., Wu, J., Zheng, M., Chen, N., Xu, K., Yan, Y., Liu, D., Zhao, D., Zhao, T., Bai, Y., Li, S., and Qi, S.: Intra-regional transport of black carbon between the south edge of the North China Plain and central China during winter haze episodes, Atmospheric Chemistry and Physics, 19, 4499-4516, https://doi.org/10.5194/acp-19-4499-2019, 2019.

Zhong, J., Zhang, X., Wang, Y., Wang, J., Shen, X., Zhang, H., Wang, T., Xie, Z., Liu, C., Zhang, H., Zhao, T., Sun, J., Fan, S., Gao, Z., Li, Y., and Wang, L.: The two-way feedback mechanism between unfavorable meteorological conditions and cumulative aerosol pollution in various haze regions of China, Atmos. Chem. Phys., 19, 3287–3306, https://doi.org/10.5194/acp-19-3287-2019, 2019.

Table 1. Correlation coefficients between hourly $PM_{2.5}$ concentrations and near-surface meteorological elements WS (wind speed), T (air temperature), P (air pressure) and RH (relative humidity) in Wuhan in January 2016.

Correlation coefficients	WS	T	P	RH
$PM_{2.5}$	0.10	0.31	-0.47	0.20

Table 2. Correlation coefficients of $PM_{2.5}$ concentrations with wind speed (WS) and air temperature (T) in different air quality levels during the study period.

Air quality	$PM_{2.5}$ levels	Number of samples	WS	T
Clean	$PM_{2.5}$ <75 μg m^{-3}	73	-0.20	0.56
Light pollution	75 μg m^{-3}≤ $PM_{2.5}$ <150 μg m^{-3}	135	-0.19	0.15
Heavy pollution	$PM_{2.5}$ ≥150 μg m^{-3}	37	0.41	-0.08

Table 3. Atmospheric static stability below heights of 200 m in the boundary layer during heavy pollution and clean air periods with the anomalies relative to the average over January, 2016 in Wuhan.

Period	heavy pollution period ($K\ km^{-1}$)	clean air period ($K\ km^{-1}$)	monthly average ($K\ km^{-1}$)
Static stability	4.4	13.2	8.6
Anomalies of stability	-4.2	4.6	-

Table 4. The relative contributions of regional transport over Central and Eastern China to three $PM_{2.5}$ heavy pollution periods P1, P2 and P3 in the YRMB with the local contributions.

Contribution rates	P1	P2	P3	Averages
Regional transport	68.1%	60.9%	65.3%	65.1%
Local contribution	31.9%	39.1%	34.7%	34.9%

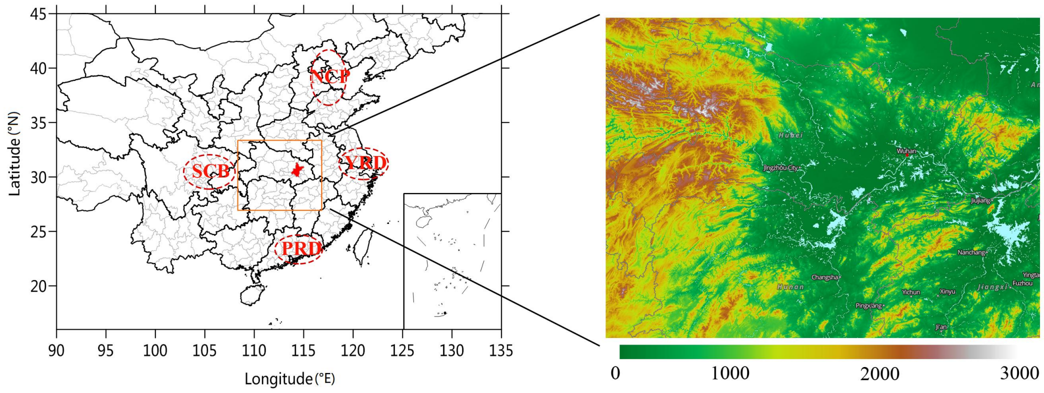

Fig. 1. (a) Distribution of the Yangtze River Middle Basin (orange rectangle) with the location of Wuhan (red area) and the major haze pollution regions of NCP, YRD, PRD and SCB in Central and Eastern China as well as (b) the YRMB region with terrain height (color contours, m in a.s.l.), the rivers and lake network (blue areas), downloaded from https://worldview.earthdata.nasa.gov.

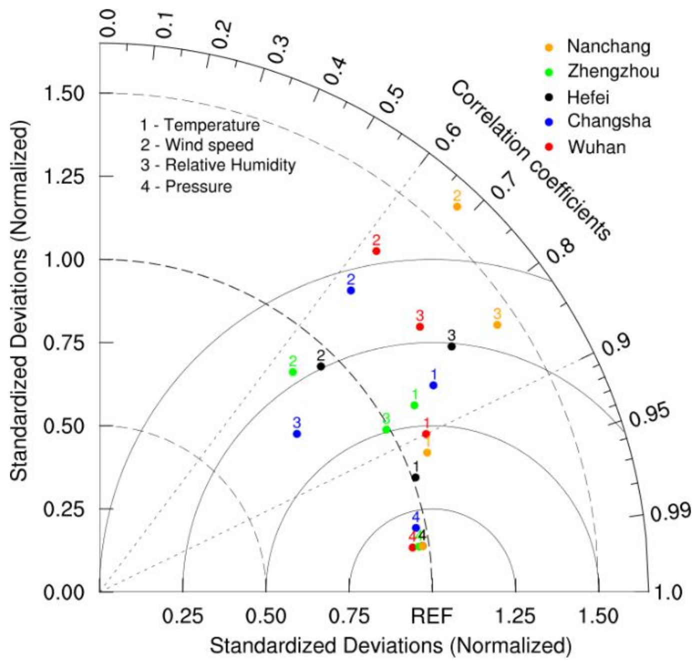

Fig. 2. Taylor plots with the normalized standard deviations and correlation coefficients between simulated and observed meteorological fields. The radian of the sector represents the correlation

coefficient, the solid line indicates the ratio of standard deviation between simulations and observations, the distance from the marker to "REF" reflect the normalized root-mean-square error (NRMSE).

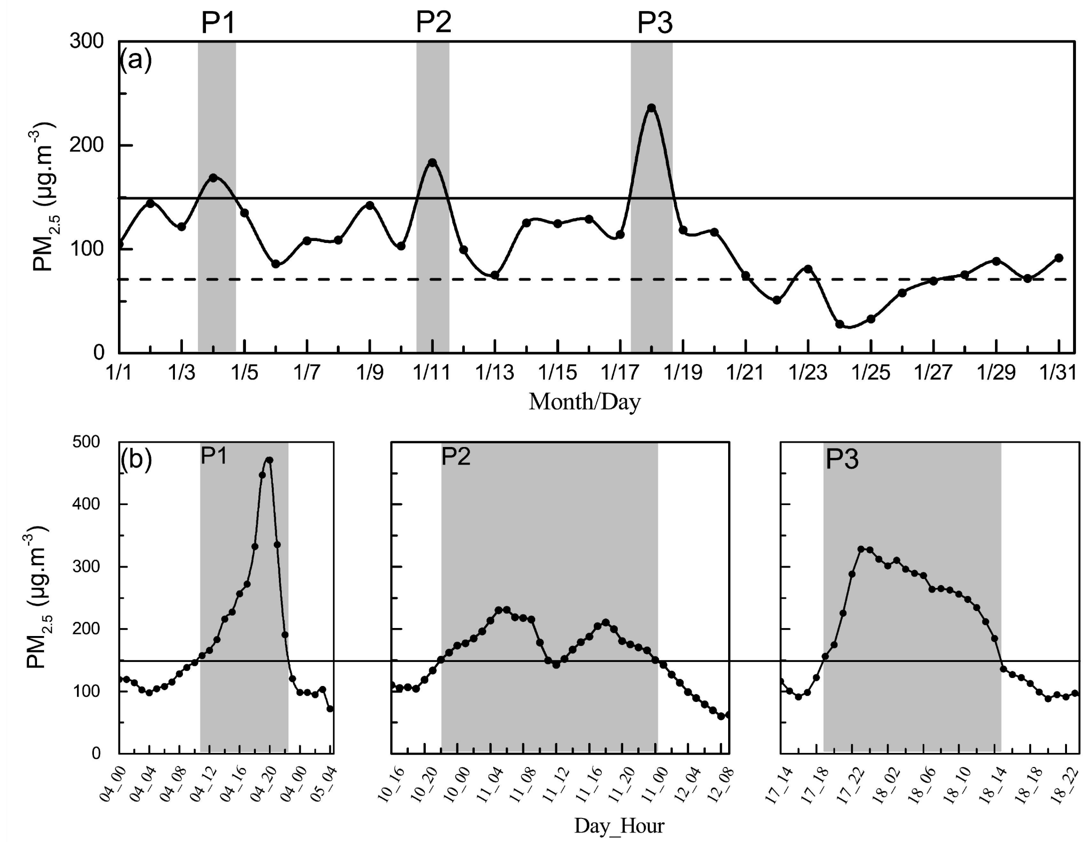

Fig. 3. (a) The daily changes of surface $PM_{2.5}$ concentrations in Wuhan in January 2016 with $PM_{2.5}$ concentrations exceeding 75 μg m^{-3} (dash line) and 150 μg m^{-3} (solid lines), respectively, for light and heavy haze pollution, and (b) the hourly variation of surface $PM_{2.5}$ concentrations in three heavy air pollution events P1, P2 and P3 with excessive $PM_{2.5}$ levels (>150 μg m^{-3}) marked by the shaded areas.

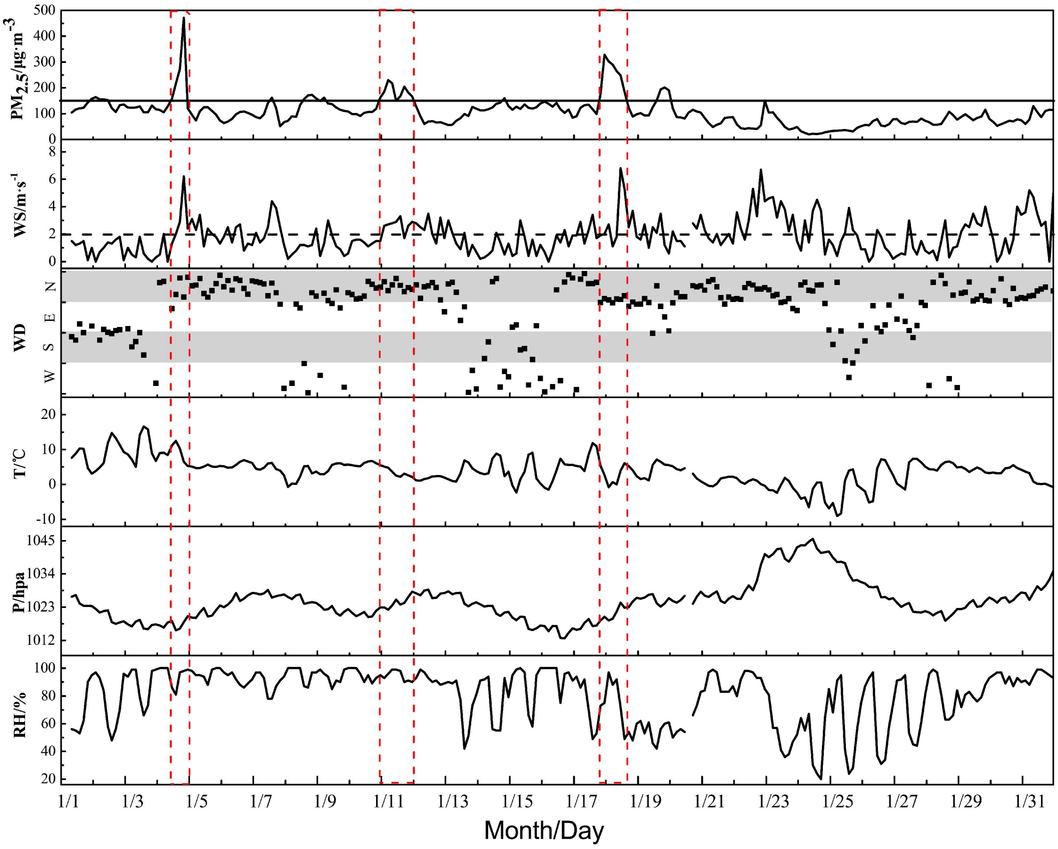

Fig. 4. Hourly variations of meteorological elements and $PM_{2.5}$ concentrations in Wuhan in January 2016 with heavy air pollution periods marked with the columns in red dash lines and $PM_{2.5}$ concentrations exceeding 150 μg m^{-3} (solid line).

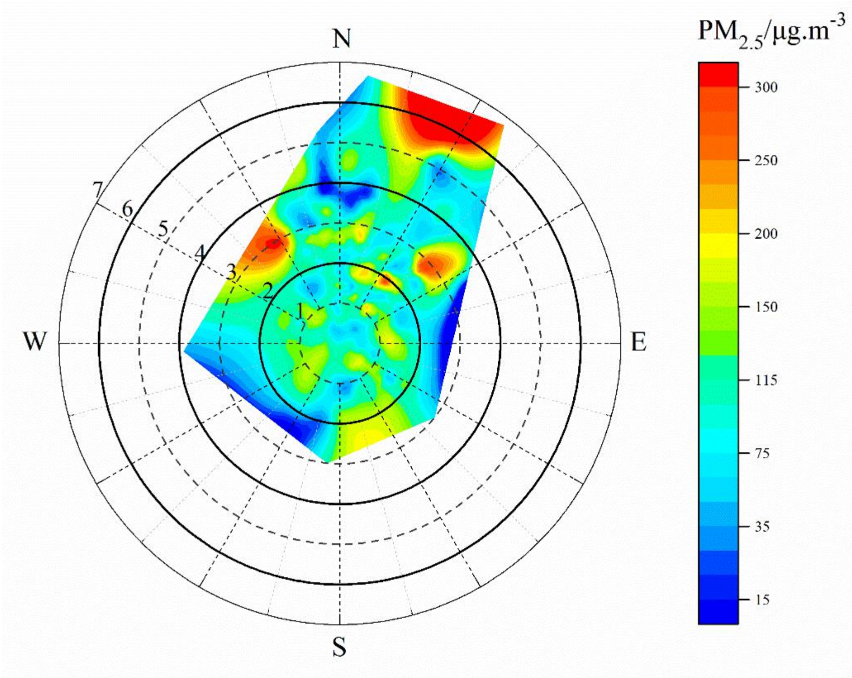

Fig. 5. A polar plot of hourly variations in wind speed (round radius, units is m s^{-1}) and direction (angles) to surface $PM_{2.5}$ concentrations (color contours, units is μg m^{-3}) in Wuhan in January, 2016.

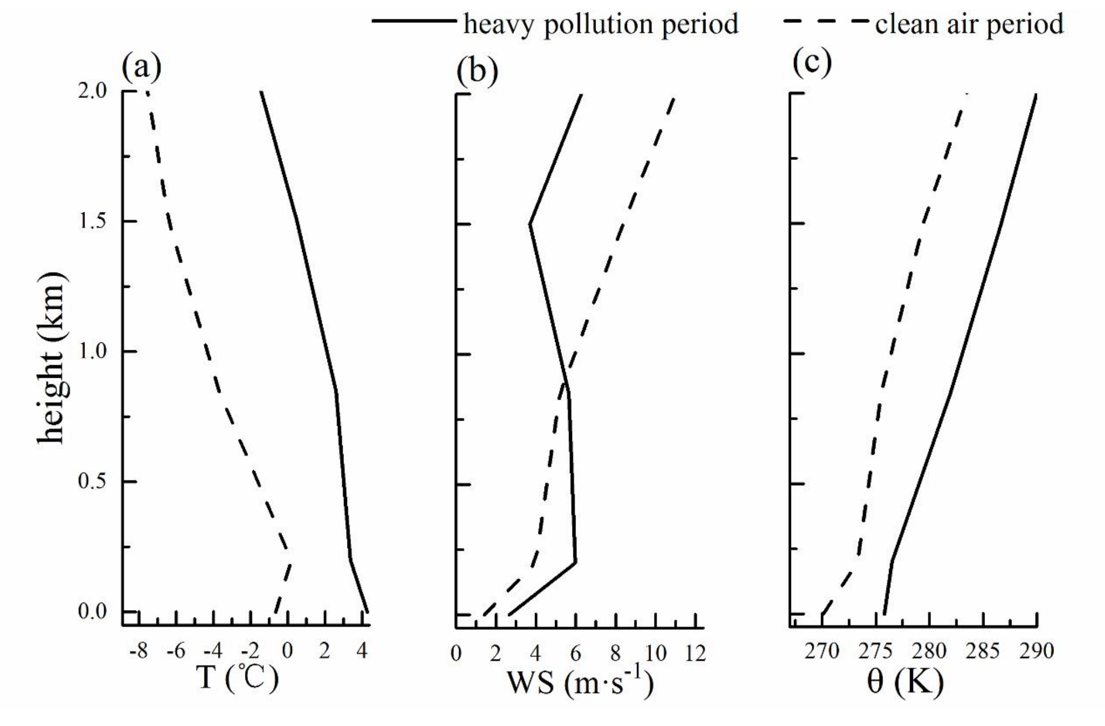

Fig. 6. Vertical profiles of (a) air temperature, (b) wind velocity and (c) potential temperature averaged in the periods of heavy $PM_{2.5}$ pollution (solid line) and clean air (dash line) over Wuhan during January 2016.

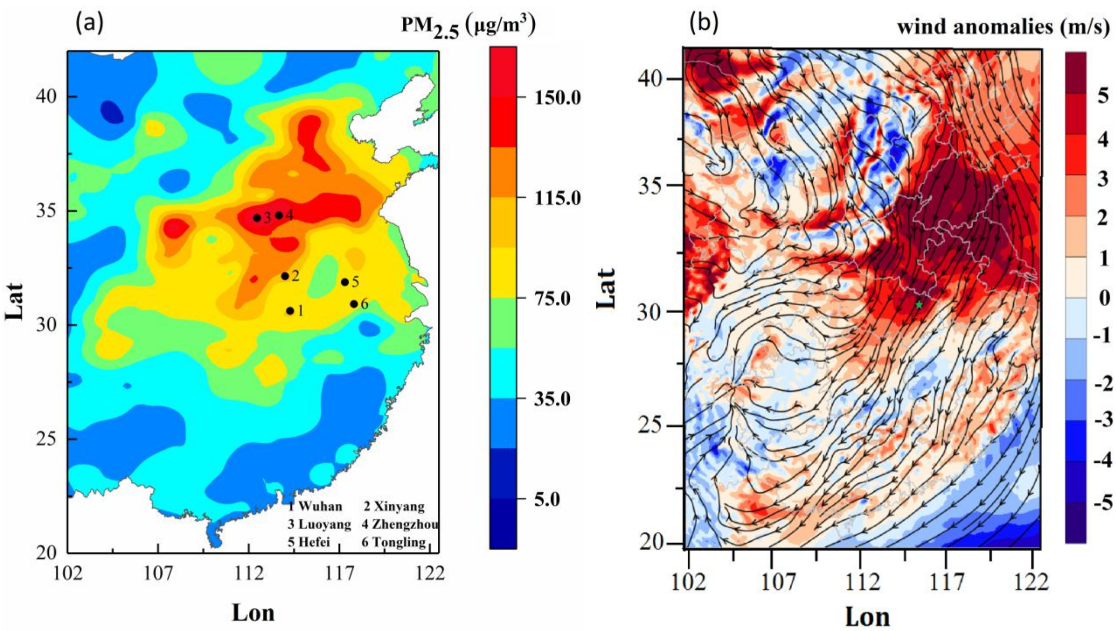

Fig. 7 Distribution of (a) monthly averages of surface $PM_{2.5}$ concentrations observed in January 2016 over CEC with the locations of six sites 1. Wuhan, 2. Xinyang, 3. Luoyang, 4. Zhengzhou, 5. Hefei and 6.Tongling as well as (b) the anomalies (color contours) of 200m wind speeds averaged during three heavy air pollution periods relatively to the monthly wind averages (streamlines) in January 2016 over CEC with the location of Wuhan (a light blue star).

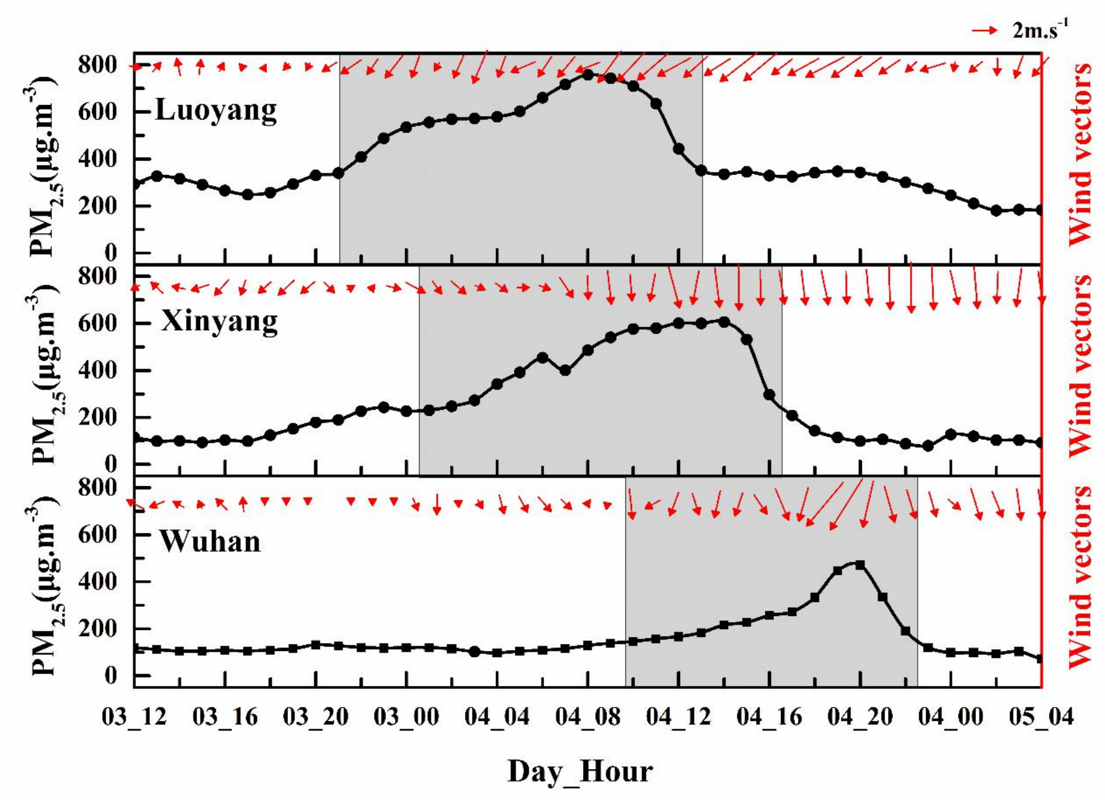
2m.s-1
Luoyang
Xinyang
Wuhan
PM2.5(μg.m-3)
Wind vectors
0
200
400
600
800
03_12
03_16
03_20
03_00
04_04
04_08
04_12
04_16
04_20
04_00
05_04
Day_Hour

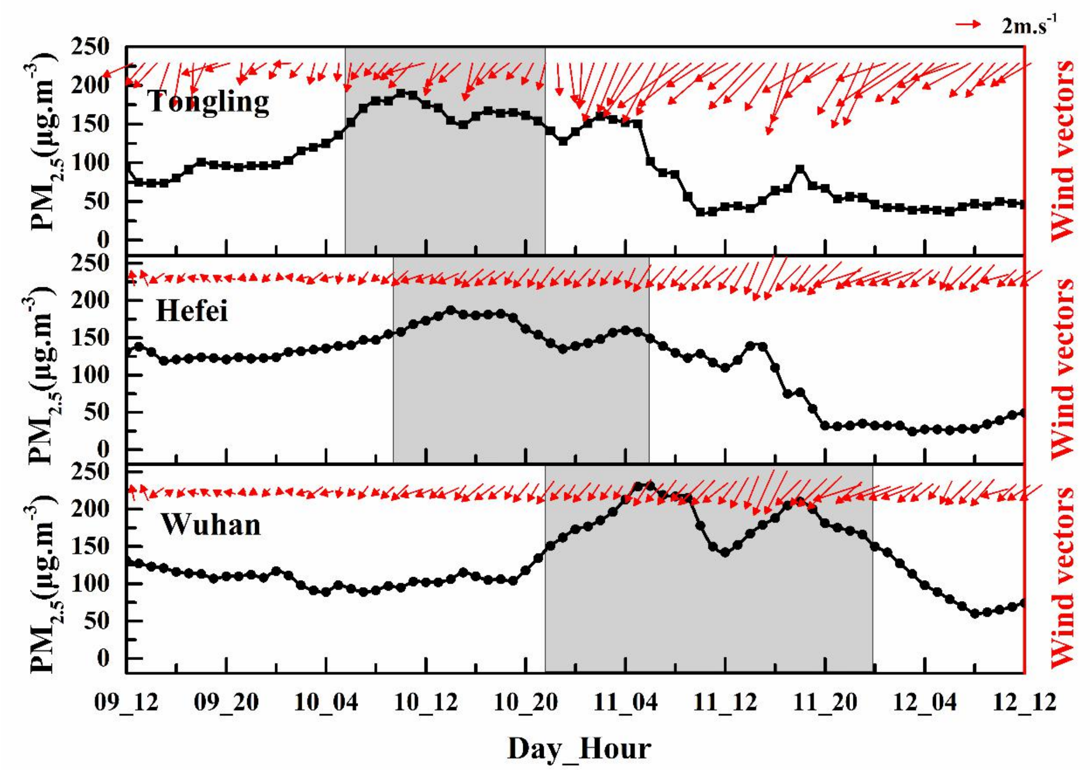
2m.s-1
Tongling
Hefei
Wuhan
PM2.5(μg.m-3)
Wind vectors
0
50
100
150
200
250
09_12
09_20
10_04
10_12
10_20
11_04
11_12
11_20
12_04
12_12
Day_Hour

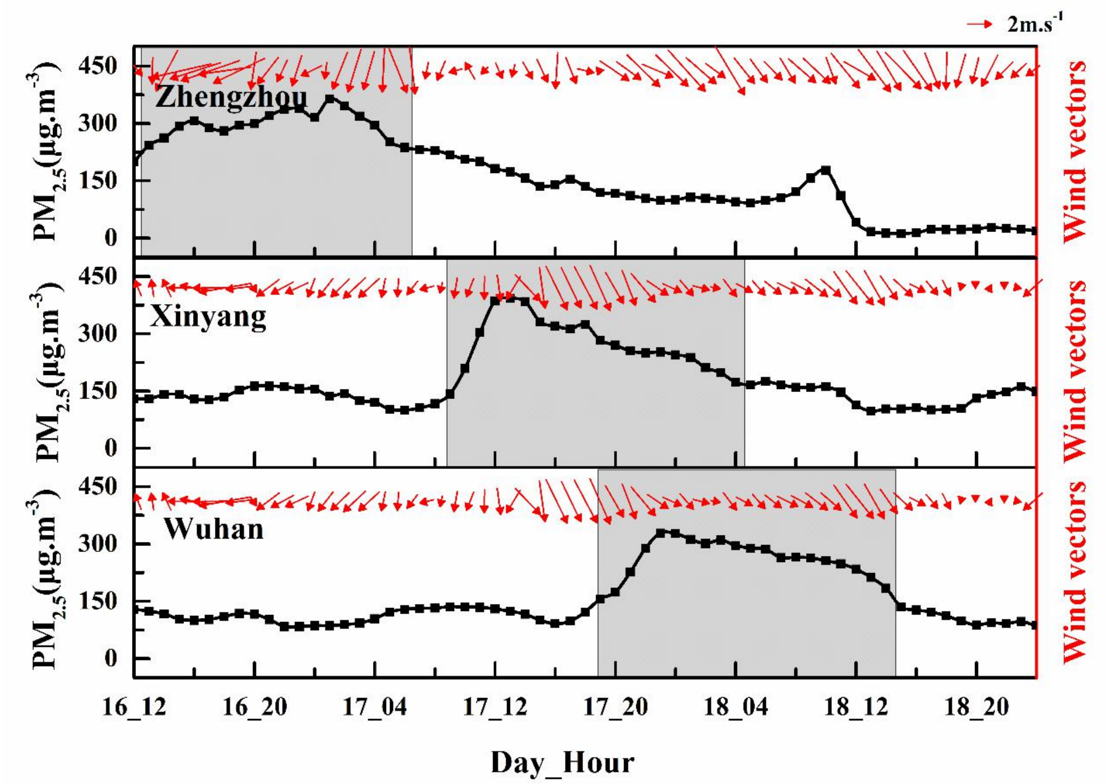

Fig. 8. Temporal changes of $PM_{2.5}$ concentrations (dot lines) and near-surface winds (vectors) observed at five upstream sites (Fig. 6) and Wuhan with shifts of $PM_{2.5}$ peaks (marked with shaded areas) to the YRMB's heavy $PM_{2.5}$ pollution periods P1 (upper panel), P2 (middle panel) and P3 (lower panel), respectively, in January 2016.

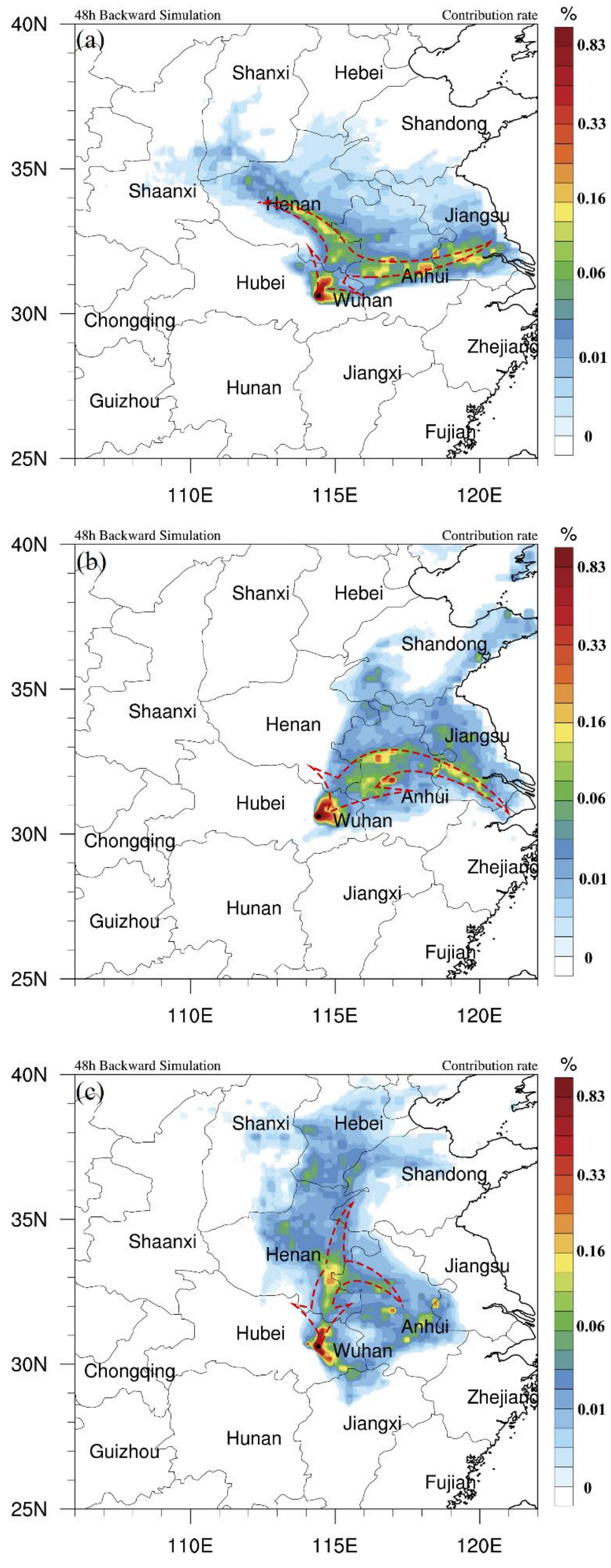

Fig. 9. Spatial distribution of contribution rates (color contours) to $PM_{2.5}$ concentrations in Wuhan

with the major pathways of regional transport over CEC (dash arrows) for (a) heavy pollution periods P1, (b) P2 and (c) P3 in January, 2016 simulated by the model FLEXPART-WRF.